Analysis of the winter and semiannual ionospheric anomalies in 1999–2009 based on GPS global International GNSS Service maps

A. Meza,[1,2] M. P. Natali,[1,2] and Laura I. Fernández[1,2]

Received 26 May 2011; revised 17 November 2011; accepted 18 November 2011; published 27 January 2012.

[1] Our work is focused on the analysis of seasonal and semiannual ionospheric anomalies using vertical total electron content (VTEC) measurements obtained by the International GNSS Service (IGS). For this study we use principal component analysis (PCA) and wavelet transform (WT) because both numerical tools allow us to isolate principal components of the VTEC variability as much spatially as temporally. The IGS VTEC maps are reorganized, and from each daily global data set, two maps were constructed: one at 12:00 LT and the other at 22:00 LT. From these two series of VTEC maps covering the period 1999–2009 for each local time, we found that the semiannual anomaly is globally recorded at noon, especially at mid and low geomagnetic latitudes, and its amplitude has a close relationship with the solar activity, and at night this anomaly is recorded during high solar activity and the larger values are located in the South American region. The values of VTEC at the March equinox exceed that of the September equinox, especially during high solar activity; the winter anomaly is recorded at noon near the geomagnetic poles region, and the effect is more important during high solar activity. At night this anomaly is present during the ascending and descending phases and minimum of the solar cycle. Thus, the night winter anomaly effect is clearly evidenced from our results.

Citation: Meza, A., M. P. Natali, and L. I. Fernández (2012), Analysis of the winter and semiannual ionospheric anomalies in 1999–2009 based on GPS global International GNSS Service maps, *J. Geophys. Res.*, *117*, A01319, doi:10.1029/2011JA016882.

1. Introduction

[2] The F_2 region has the greatest concentration of electrons, and it is also the region of greatest interest in radio propagation; but it has the characteristic that it is the most variable, the most anomalous and the most difficult region to predict. In terms of the theory of *Chapman* [1931], which is based on the electron concentrations varying regularly with solar zenith angles, the F_2 region is anomalous in many ways. There are many well-known anomalies in the F_2 layer. Several authors have analyzed these variations and have identified three major components: winter maximum (seasonal), equinoctial maxima (semiannual) and a component which peaks in December–January (annual). In this work we will focus on the two first kinds of effects.

[3] The winter (seasonal) anomaly has a large daytime electron density in winter compared to summer. *Rishbeth and Setty* [1961] proposed that the seasonal variation of N_mF_2 is related to changes of composition. *Johnson* [1964] suggested that this change was a result of summer hemisphere being heated and the lighter neutral constituents being convected to the winter hemisphere. *Torr and Torr* [1973] explained this variation in terms of the winter/summer thermospheric composition ($[O]/[N^2]$) change including vibrationally excited nitrogen. The winter anomaly falls off in amplitude and area with decreasing solar activity as would be expected to happen with decreasing energy input and consequent reduction in the convection activation mechanism. The daytime seasonal anomaly is strong in the bottomside ionosphere and extends up to about 400 km altitude. *Zhao et al.* [2007] have shown that the seasonal anomaly is more significant near the pole region.

[4] At night the winter anomaly disappears; this is due to the effect of the strong nighttime equatorward wind in the summer hemisphere and the values of electron density in summer far exceeding those in winter, especially at altitudes above 200 km and high solar activity. Meanwhile in low solar activity, *Jakowski and Förster* [1995] found a Nighttime Winter Anomaly (NWA) effect at the midlatitude ionosphere in the American and Asian longitude sectors using the information of the Total Electron Content (TEC), vertical sounding data as well as topside sounder measurements onboard Alouett. They concluded that NWA could be explained by interhemispheric coupling via plasma fluxes along magnetic flux tubes. *Mikhailov et al.* [2000] and *Farelo et al.* [2002] found two peaks when studying the N_mF_2 night variability. Both peaks, during premidnight and

[1]Facultad de Ciencias Astronómicas y Geofísicas, Universidad Nacional de La Plata, La Plata, Argentina.
[2]Consejo Nacional de Investigaciones Científicas y Técnicas, Buenos Aires, Argentina.

0148-0227/12/2011JA016882

postmidnight, show different features linked to the different physical mechanisms responsible for their formation. They asseverated that the premidnight peaks in winter are due to a strong equatorward thermospheric wind raising the F_2 layer to heights with the lower recombination rate.

[5] The semiannual anomalies, i.e., the semiannual maximum variations of N_mF_2, are recorded near the equinoxes. They are large every year, especially at middle and low latitude. *Yonezawa* [1971] proposed that the semiannual variation of N_mF_2 is related to the variation of the upper atmosphere temperature. *Torr and Torr* [1973] suggested that this is due to semiannual variation in neutral densities associated with geomagnetic and auroral activity. *Mayr and Mahajan* [1971] showed that the semiannual effect appears as a persistent feature of the ionosphere which is not related to fluctuations in the 10.7 cm noise or the EUV radiation. This gives support to theories that attribute the semiannual effect to variations in the lower atmosphere. Although theoretically predicted temperature variations [*Volland*, 1969] could quantitatively account for the observed semiannual variations in the height of the F_2 peak, the variations in N_mF_2 require additionally significant variations in the neutral composition at lower heights and evidence for this is found in rocket-borne [O]/[O_2] measurements at 120 km. *Millward et al.* [1996], using the coupled thermosphere-ionosphere-plasmasphere model (CTIP), found the semiannual variation in N_mF_2 noontime, a common feature of the F_2 layer, particularly at low latitudes and in the southern hemisphere at midlatitudes. Results from the model reveal such a variation, is the most prominent at midlatitudes in the South American sector and concluded that this phenomenon is intimately related to the large offset of the geomagnetic axis from Earths spin axis in the southern hemisphere. *Lal* [1995] constructed a planetary index of the critical frequency of F_2 layer; it showed marked semiannual maxima around the equinoxes, in a similar way to that of the *Dst* geomagnetic index (which measure the intensity of the ring current). Consequently, he discussed the relation of the solar wind energy to these processes [*Lal*, 2000]. *Ma et al.* [2003] suggested that the semiannual variation of the diurnal tide in the lower thermosphere induces the semiannual variation of the amplitude of the equatorial electrojet. This causes the variation of the amplitude of the ionospheric equatorial anomaly through a fountain effect and this process induces the semiannual variation of N_mF_2 at low latitude. The semiannual variations appear around the globe in daytime, and except in low-latitude regions and in South America sector, there is no obvious semiannual variation of N_mF_2 in the nighttime [*Li and Yu*, 2003]. The amplitude of this variation has close relationship with the solar activity (larger values in maxima of solar activity). They have asymmetrical structures between the two Hemispheres and at different longitudes [*Ma et al.*, 2003]. *Balan et al.* [2000] found a strong equinoctial asymmetry that exists near the ionospheric peak and above at all local times with the values of N_mF_2 in March equinox exceeding those of September equinox by up to 50%.

[6] In May 1998 IGS created the Ionosphere Working Group [*Feltens and Schaer*, 1998]. Among the scientific groups and institutes that are presently dedicated to ionospheric studies using GPS observations three of them can be distinguished as the most important: the Center for Orbit Determination in Europe (CODE), that belongs to the Astronomical Institute of the University of Bern, Switzerland (http://www.aiub.unibe.ch/igs.html); the NASA Jet Propulsion Laboratory (JPL) (http://iono.jpl.nasa.gov/), Pasadena, USA; and the Astronomy and GEomatics group (gAGE) (http://gage1.upc.es/), Barcelona, Spain. The Global Ionospheric Maps (GIMs) computed by each group are made available for the users as a file in the IONosphere map EXchange (IONEX) format [*Schaer et al.*, 1998]. The file contains all the information relative to the computation process and the VTEC information is presented in the form of a grid of 2.5 degrees in latitude and 5 degrees in longitude.

[7] Many researches using GPS observations have focused on the study of local and regional characteristics of ionospheric anomalies [*Huang and Cheng*, 1996; *Unnikrishnan et al.*, 2002; *Wu et al.*, 2004; *Meza and Natali*, 2008]. *Mendillo et al.* [2005] have found the annual anomaly in TEC to be a global characteristic by using GIMs data, and their analysis was extended by *Zhao et al.* [2007], exploring the global features of the other anomalies (winter and semiannual anomalies).

[8] The TEC might have different characteristics as compared with those derived from the N_mF_2. That means that if the anomaly in topside ionosphere is very strong as compared with the bottomside ionosphere, the anomaly will be stronger for the TEC than for the N_mF_2 [*Zhao et al.*, 2007].

[9] The aim of this work is the analysis of the semiannual and seasonal effects in TEC during a solar cycle period (1999–2009) at noon and at night. Spatial and temporal ionospheric variability are investigated from Global IGS VTEC maps applying principal component analysis (PCA). For time variations wavelet tools are used.

2. Methodology

[10] The IONEX format allows the storage of snapshots of the electron density (including associated RMS information) referring to particular epochs and to a two- or even three-dimensional, Earth-fixed grid. IONEX data supply a good estimation of the worldwide VTEC. These data provide VTEC values around the world at intervals of 2.5 degrees in latitude and 5 degrees in longitude.

[11] Global IGS VTEC maps during solar cycle 23 (1999–2009) are used in this work. These VTEC maps show a global snapshot of the ionosphere every 2 h. Therefore, the main geographical VTEC variation that can be seen on them is the ionization due to solar radiation. Since we are not interested in analyzing that effect but the ionospheric response to similar solar radiation conditions on different locations, we reorganized the VTEC data as follows: Two different solar radiation conditions were selected for analysis: from each daily global data sets, composed by twelve VTEC maps, two maps were constructed at two different local times: 12:00 and 22:00 LT. The temporal series were constructed in the following ways.

[12] 1. Assuming that the ionosphere does not change in a 2 h window, we took 30 degree slices from all VTEC maps for each day, centered on the same local time. These slices were then merged into a new VTEC map according to their central longitude. This procedure resulted in two new VTEC maps per day, corresponding to the two different local times selected. The complete data set consists of two series of

VTEC maps covering the period 1999–2009 for each local time of our analysis. The difference between VTEC and the temporal VTEC average of every grid point are computed. Such differences, called VTEC residues ($VTEC_{ra}$) are estimated as is required for the PCA technique implementation.

[13] 2. Fourier series are used on VTEC residues to filter the solar cycle and the half solar cycle [*Mursula et al.*, 1997]. The $VTEC_{ra}$ are fitted using Fourier series, so the amplitude and phase for solar cycle and half solar cycle are computed. From these results the $VTEC_{ra}$ modeled are obtained, called $VTEC_{r\text{-}model}$. Then, new residuals are computed from the difference between $VTEC_{ra}$ and $VTEC_{r\text{-}model}$. This filter was applied separately for each latitude-longitude grid point.

[14] *Djurović and Pâquet* [1996] claimed to have found an oscillation with a period of about 5.5 years in several solar and solar-terrestrial parameters, in particular in solar activity as indicated by sunspot numbers. *Mursula et al.* [1997] analyzed the temporal evolution of solar activity and have examined *Djurović and Pâquet* [1996] results in detail. They showed that their conclusion is based on an artifact due to a questionable method applied, and due to the asymmetric form of the solar cycle. So, there is no reasonable evidence for the existence of a fundamental 5.5 year periodicity in solar activity. From these results all parameters that are affected by the fundamental 11 year solar cycle will depict a nonzero residual dominated by the second harmonic. In order to avoid the artifact periodicity, the VTEC residues are filtered by solar cycle and the half solar cycle.

2.1. PCA Application

[15] PCA is used to identify spatial structures that have dominant contribution to the total variability together with their time evolution. PCA is well suited for the analysis of multivariate time series. One main reason for that is that the technique can be used to identify spatial structures that have dominant contribution to the total variability together with their time evolution without the need to propose any particular a priori functional model.

[16] PCA is used to express a correlated data set on a new orthonormal base of minimum dimension. The shape of the base functions is determined from the data set itself. This method is of special interest when the phenomena under study are not necessarily a superposition of well-known simple components that would point other techniques (e.g., Fourier analysis) as more adequate.

[17] Let z(t, x) be VTEC measures, at point x (latitude and longitude) in the atmosphere at time t. Let these measurements be taken over the set of locations x = 1,.. …, p at times t = 1, … …, n. The first step in PCA is to center the time series on their time averages. This is,

$$\mathbf{z}'(t,x) = \mathbf{z}(t,x) - \bar{\mathbf{z}}(t,x) \tag{1}$$

with

$$\bar{\mathbf{z}}(t,x) = \frac{\sum_{t=1}^{n} \mathbf{z}(t,x)}{n} \tag{2}$$

These collections can be thought as p × 1 (i.e., column) vectors z′(t) = {z′(t, 1), … .., z′(t, p)} forming a swarm of points about the origin of a p-dimensional Euclidean space (Ep). Now it is possible to construct the symmetric scatter matrix, S, in Ep.

$$\mathbf{S} = \sum_{t=1}^{n} \mathbf{z}'(t)\mathbf{z}'^{T}(t) \tag{3}$$

This matrix has a set of p orthonormal eigenvectors $\mathbf{e}_j$. From these $\mathbf{e}_j$ we can construct the principal components (or amplitudes) of the data set, $\mathbf{a}_j(t)$:

$$\mathbf{a}_j(t) = \sum_{x=1}^{p} \mathbf{z}'(t,x)\mathbf{e}_j(x) = \mathbf{z}'(t)^{T}\mathbf{e}_j \text{ (Analysis of } \mathbf{z}') \quad t = 1,\ldots,n \quad ; j = 1,\ldots,p \tag{4}$$

These $\mathbf{a}_j(t)$, can be thought of as a family of time series $\{\mathbf{a}_j(t)$: t = 1,…, n$\}$. The most important property of these time series is that they are mutually uncorrelated, carrying information about the variance of the data set along the directions $\mathbf{e}_j$.

[18] Finally, and most importantly, the original centered data set can be exactly represented in the form

$$\mathbf{z}'^{T}(t,x) = \sum_{j=1}^{p} \mathbf{a}_j(t)\mathbf{e}_j^{T}(x) \text{ (Synthesis of } \mathbf{z}') \quad t = 1,\ldots,n; \quad x = 1,\ldots,p. \tag{5}$$

By eigenvalue decomposition of the covariance matrix of VTEC variations the PCA technique identifies those spatial structures of the ionospheric variability that have dominant contribution to the total variance. The spatial structure of the ionospheric variability is represented by the eigenvector ($\mathbf{e_j}$) and its temporal evolution is described by a series of coefficients ($\mathbf{a_j}$), called principal components. Eigenvector and principal components together are called mode. Modes are ordered according to decreasing eigenvalues, such the first mode represents the largest part of the variance, the next mode the second largest part, etc. This method is a powerful tool because the principal components have the information of the original data, which means, the orthonormal functions are directly determined by the data itself. For further details of the foundations and methodology applied in this work see *Preisendorfer* [1988] and *Meza and Natali* [2008].

2.2. Wavelet Transform

[19] Wavelet technique has been chosen to measure the time-frequency variations of spectral components on the amplitude time variation obtained by PCA ($\mathbf{a_j}$(t)). The application of the wavelet transform (WT) as a time-frequency analysis method is inherent in its ability of providing information not only about the frequency of the event but also about its location in the time series. The WT refers to an integral transform using wavelets as integration kernels for analysis to extract information about the process [*Kumar and Foufoula-Georgiou*, 1997]. An extensive overview of the WT properties and their common geophysical applications can be found in [*Daubechies*, 1992; *Kumar and Foufoula-Georgiou*, 1994, 1997; *Holschneider*, 2000].

[20] Defining the Morlet mother wavelet as

$$\psi(t) = \frac{e^{i\omega_0 t}}{\sqrt[4]{\pi}\, e^{t^2/2}} \tag{6}$$

where t is time and ω_0 is set equal to 6 to fulfill the admissibility condition. A family of wavelets is generated from equation (6) by scaling and translating the mother wavelet. Thus, a family of Morlet wavelets is:

$$\psi_{s,b}(t) = \frac{1}{\sqrt{s}}\psi\left(\frac{t-b}{s}\right) \quad (7)$$

where b denotes the shift parameter; s the scale and the normalization factor $s^{-1/2}$ guarantees equal energy at different scales [*Ge*, 2007]. The continuous Morlet WT of a discrete equal time space data series $x(t)$ is defined as the convolution of the data series with the family of the Morlet wavelets [*Kumar and Foufoula-Georgiou*, 1997; *Torrence and Compo*, 1998].

$$WT(s,b) = \int_{-\infty}^{\infty} x(t)\psi^*_{s,b}(t)dt \quad (8)$$

where (..)* refers to the complex conjugate. Because the WT is an inner product between an analyzing wavelet at a given scale and the signal, the wavelet coefficients will combine information about both the signal and the wavelet [*Farge*, 1992]. In a discrete form, the expression for the wavelet coefficient at time index n and scale s is [*Torrence and Compo*, 1998; *Ge*, 2007].

$$W(s) = \sum_{n'=0}^{N-1} x(n')\psi^*\left[\frac{(n'-n)\delta t}{s}\right] \quad (9)$$

where N is the length of the data time series and δt is the sampling period.

[21] After choosing the mother wavelet, the set of convolution products of equation (9) must be solved. It is common to perform them in Fourier space using FFT (Fast Fourier Transform).

[22] Provided that the selected mother wavelet is Morlet, thus the wavelet transform will also be complex. In order to avoid dealing with the separate analysis of the real and imaginary parts, we will use the wavelet power spectrum, i.e., the squared modulus of the wavelet transform ($|W(s)|^2$) [*Torrence and Compo*, 1998].

[23] The confidence of the WT results is given by the cone of influence, which delimits the region where the errors of the edge effects are important. Any pick out of the cone of influence have to be dismissed. The edge effect is a consequence of the zero padding of the time series.

[24] In order to analyze fluctuations in power over a band of scales, we used the scale-averaged wavelet power spectrum (SAWPS) as defined by *Torrence and Compo* [1998].

$$\bar{W}_n^2 = \frac{\delta j\,\delta t}{0.776}\sum_{j=j1}^{j2}\frac{|W(s_j)|^2}{s_j} \quad (10)$$

where δj is a factor related to the width in spectral space of the wavelet mother function: it is the space between discrete scales. Small values of δj provide a good resolution, effectively, the smaller the δj is the better the scale resolution is [*Torrence and Compo*, 1998]. Notice that equation (10) is the weighted sum of the wavelet power spectrum over scales s_1 to s_2.

[25] The mean Carrington rotation period of about 27 d [*Ulrich and Boyden*, 2006] on the amplitude time variation obtained by PCA was removed by smoothing the time series with a low-pass Vondrak filter [*Vondrák*, 1977]. The applied removed the 95% of the signal at periods lower than 80 d.

[26] The PCA amplitudes residuals after filtering were the input data time series for the WT. Following, the SAWP spectrum was computed over two different bands: 0.4–0.6 year to show the semiannual variability and 0.9–1.1 year to show the annual variability.

3. Results

[27] The VTEC behavior is studied from 1999 to 2009, for local noon and night. These epochs correspond to two different times of series once the VTEC grids are built for every day and every year. PCA analysis was applied to each time series in order to estimate the amplitudes ($\mathbf{a_j}$) and eigenvectors ($\mathbf{e_j}$) associated with each data set (equations (4) and (5)).

[28] For this data set, we found that the first two PCA modes contain 80% of the total VTEC variability. Modes 1 and 2 can be written as the products ($\mathbf{a_1}.\mathbf{e_1}$) and ($\mathbf{a_2}.\mathbf{e_2}$), respectively, where $\mathbf{e_j}$ contain the spatial variation and the $\mathbf{a_j}$ contain the temporal variation of the data set. $\mathbf{e_j}$ and $\mathbf{a_j}$ are adimensional, the units of the product of $\mathbf{e_j}$ and $\mathbf{a_j}$ are TECU (1 TECU = 10^{16}electron/m^2). Thus, there are 4 PCA amplitude data time series: mode 1 and mode 2 at 12:00 LT; mode 1 and mode 2 at 22:00 LT.

[29] Then, in order to remove the mean solar rotation period, a Vondrak filter was applied to each PCA amplitude time series ($\mathbf{a_j}$). Each of them has 3935 equally spaced samples at 1 d period. For limiting the edge effect, each time series was zero padded to bring their length to the next power of two. Below we compute the wavelet power spectrum of these four times series.

[30] The results of the application of the two statistical processes on VTEC data are shown in Figures 1–4. Because we analyzed mode 1 and mode 2 at local noon and night, there are four figures, one for each mode and local time.

[31] Each figure is a composite panel of six plots formed by the PCA eigenvector variability ($\mathbf{e_j}$) (Figures 1a–4a); the PCA amplitude variability ($\mathbf{a_j}$) (Figures 1b–4b); the PCA amplitude time series after the mean Carrington period was removed (Figures 1c–4c, top); the wavelet power spectrum of the filtered PCA amplitudes (Figures 1c–4c, bottom); the SAWPS (equation (10)) over the band 0.4–0.6 year (Figures 1d–4d) (these values were computed from the wavelet power spectrum shown in Figures 1c–4c); and the SAWPS (equation (10)) over the band 0.9–1.1 year (Figures 1e–4e) (these values were computed from the wavelet power spectrum shown in Figures 1c–4c).

[32] The plot of each wavelet power spectrum of the filter PCA amplitude (Figures 1c–4c) has a thick line that encloses regions of greater than 95% confidence level for white noise. The dotted line shows the cone of influence caused by the zero padding of the time series. Any peak of the power spectrum falling in this area should not be considered in the analysis presumed of being an artifact of the edge effects.

[33] Thus, we will present the VTEC variability analysis divided into the two different local times. For 12:00 LT (Figures 1 and 2), the first mode shows strong semiannual

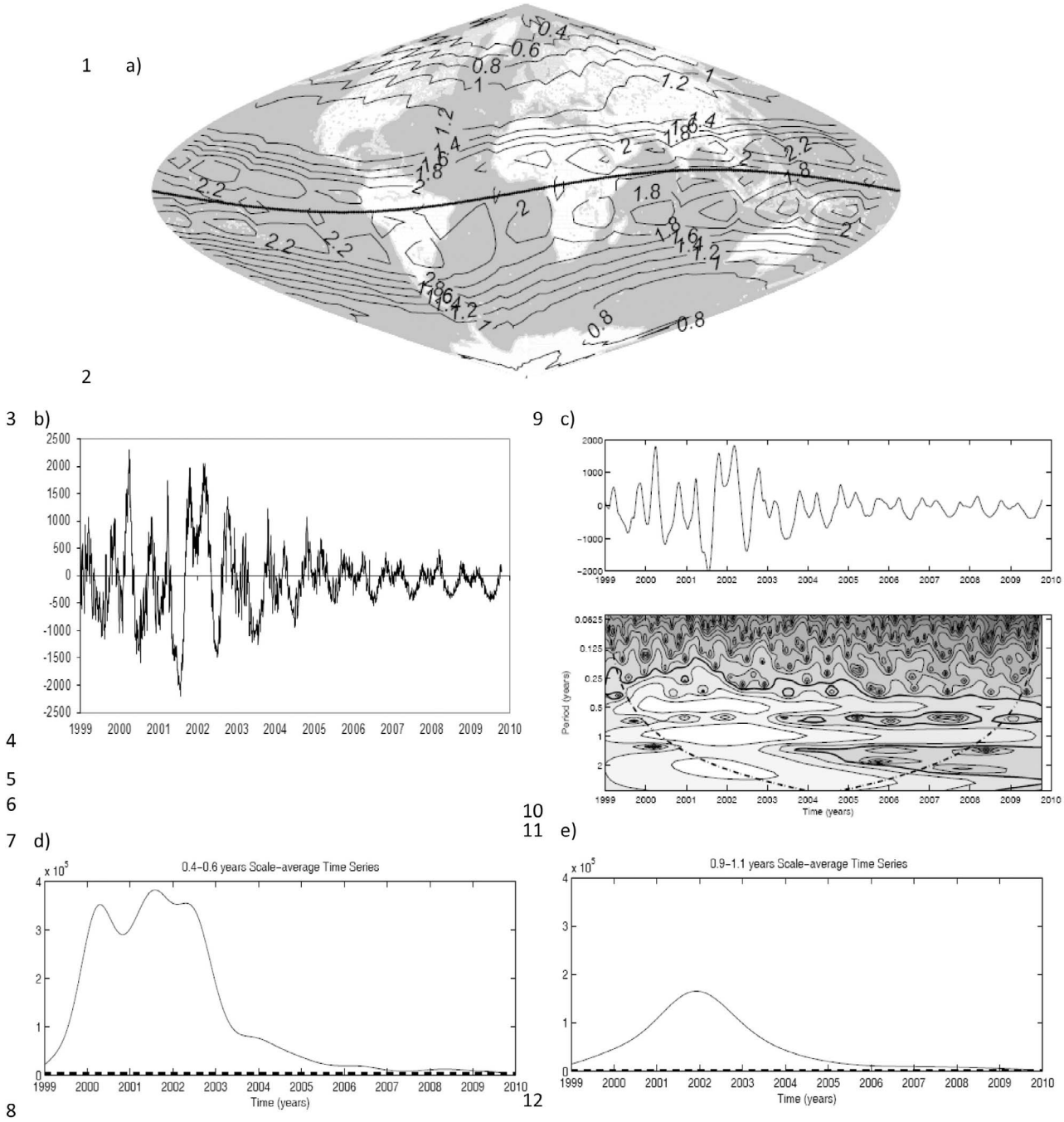

Figure 1. (a) Spatial variation in the first mode at noon. (b) Time variation in the first mode at noon. The x axis is the day of year (DOY) and the y axis is the amplitude multiplied by a factor of 10^{-2}. (c) Wavelet power spectrum of the time variation residuals after mean Carrington period removal. (d) Scale-averaged wavelet power over the 0.4–0.6 year band. (e) Scale-averaged wavelet power over the 0.9–1.1 year band.

component; the contribution to the variance is 75%. From Figure 1a the semiannual anomaly is two times larger at equatorial low geomagnetic latitude than at high latitude. At mid geographic latitude the variation is larger in the Southern Hemisphere than in the Northern Hemisphere, especially in the South American region. The amplitude of this effect is larger at high solar activity than at low solar activity (Figure 1b). The maximum peak is recorded preferably in March equinox than in September equinox. The variability of VTEC in March equinox exceeds September equinox by up to 40% during high solar activity.

[34] From the wavelet power spectrum is easy to see that the annual and semiannual effects show remarkable maximums (Figure 1c). From the SAWPS we can see that the semiannual effect is the most important contribution during the whole period (Figure 1d), but especially in high

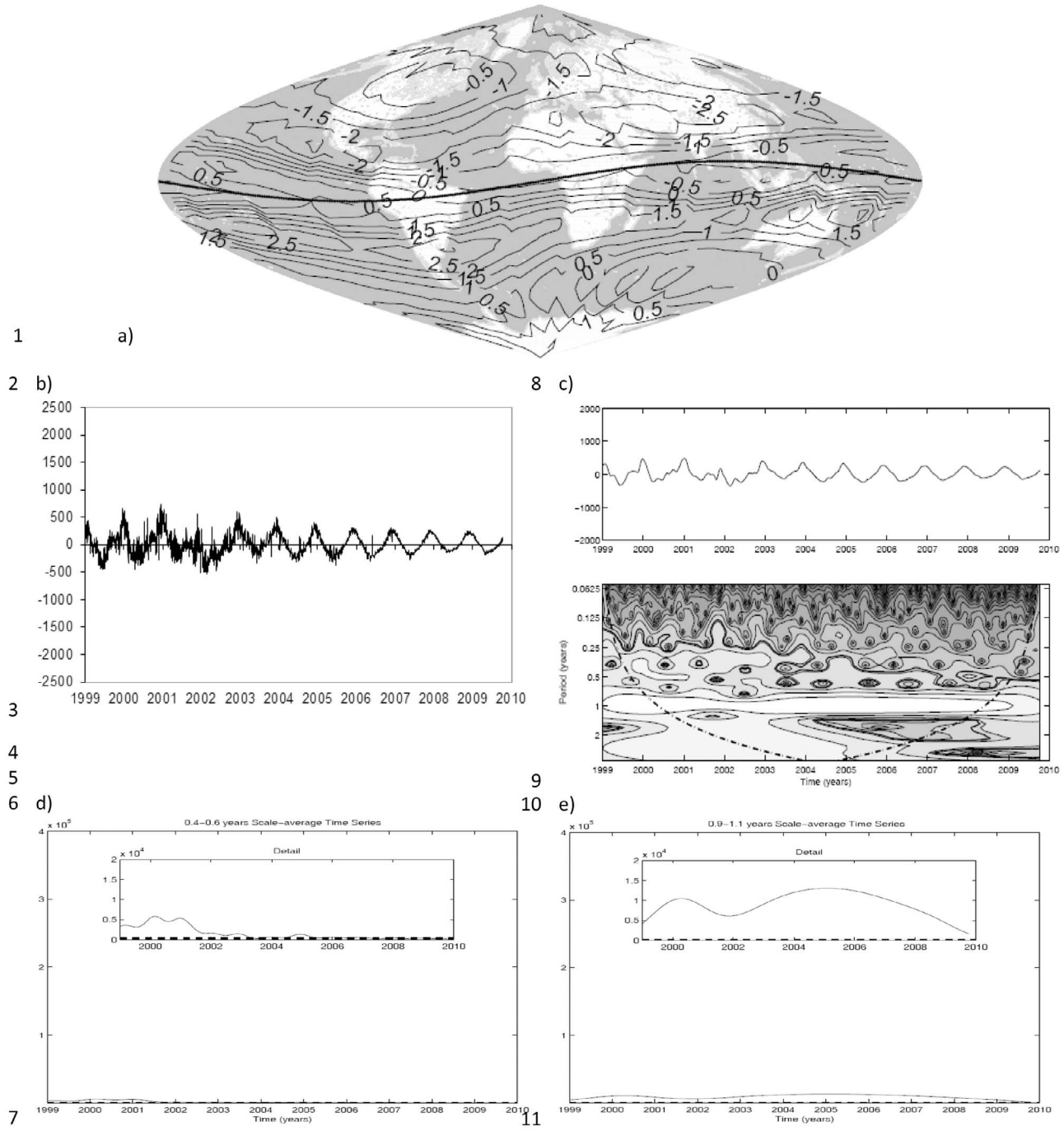

Figure 2. (a) Spatial variation in the second mode at noon. (b) Time variation in the second mode at noon. The x axis is the DOY and the y axis is the amplitude multiplied by a factor of 10^{-2}. (c) Wavelet power spectrum of the time variation residuals after mean Carrington period removal. (d) Scale-averaged wavelet power over the 0.4–0.6 year band. (e) Scale-averaged wavelet power over the 0.9–1.1 year band.

solar activity and the descending cycle. Besides, regarding Figures 1d and 1e, they show that both effects annual and semiannual are comparable during low solar activity.

[35] The second mode (7% of the variance contribution) shows variation with maximum values in summer solstice and minimum in winter solstice except near the geomagnetic pole region where the winter anomaly is present (Figure 2a). From Figures 2b and 2c, there is an evident annual variation. Both SAWPS computation (0.4–0.6 year band and 0.9–1.1 year band) for the filtered PCA amplitude of the mode 2 at local noon are negligible. Figures 2d and 2e show at top the same time series but zoomed one order of magnitude. From these details one can see that the annual anomaly is more important at the ascending and descending phases of the solar cycle.

[36] From Figure 3a (for 22:00 LT, Figures 3 and 4) the variation is larger at mid to low geomagnetic latitudes and maximum values are recorded in the South American region.

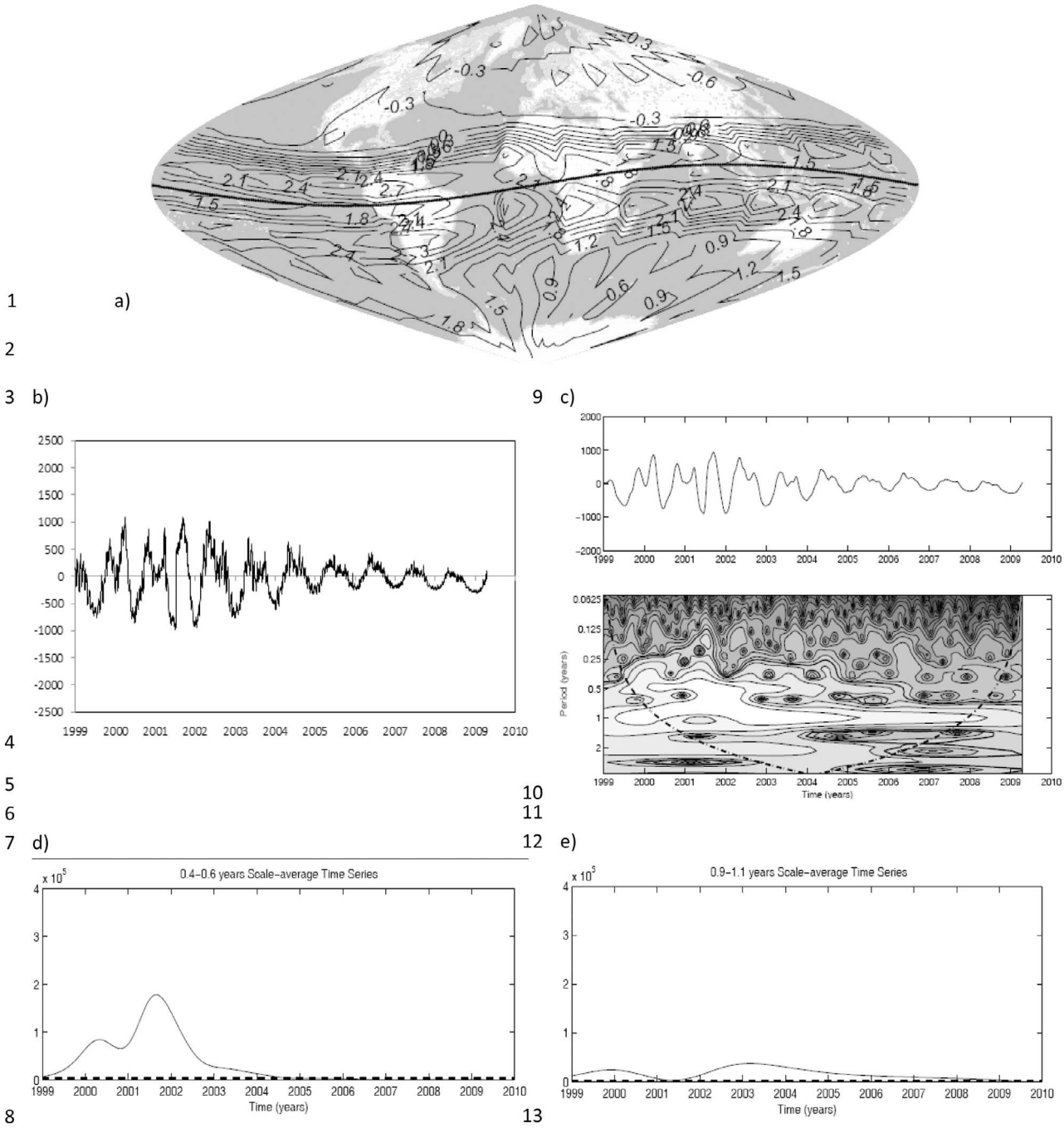

Figure 3. (a) Spatial variation in the first mode at night. (b) Time variation in the first mode at night. The *x* axis is the DOY and the *y* axis is the amplitude multiplied by a factor of 10–2. (c) Wavelet power spectrum of the time variation residuals after mean Carrington period removal. (d) Scale-averaged wavelet power over the 0.4–0.6 year band. (e) Scale-averaged wavelet power over the 0.9–1.1 year band.

The first mode also shows semiannual and annual variation (Figures 3b and 3c) and the contribution to the variance is 51%. The variability of VTEC in March equinox exceeds September equinox by up to 30% during high solar activity.

[37] Figures 3b and 3d show equinoctial maximum during high solar activity. Moreover, the semiannual variation (Figures 3b and 3d) is observed in the equatorial region and the Southern Hemisphere (Figure 3a). During low solar activity the annual variability is the most important (Figures 3b and 3e), showing an annual anomaly with maximum values in July and minimum in December for Southern Hemisphere and vice versa for Northern Hemisphere at mid and high geographic latitudes (Figure 3a).

[38] The second mode contribution to the variance is 27% and the variation is the largest at mid geomagnetic latitude (Figure 4a). As before, the second mode shows annual and semiannual variability (Figures 4b and 4c). From Figures 4d and 4e the semiannual component has larger values than the

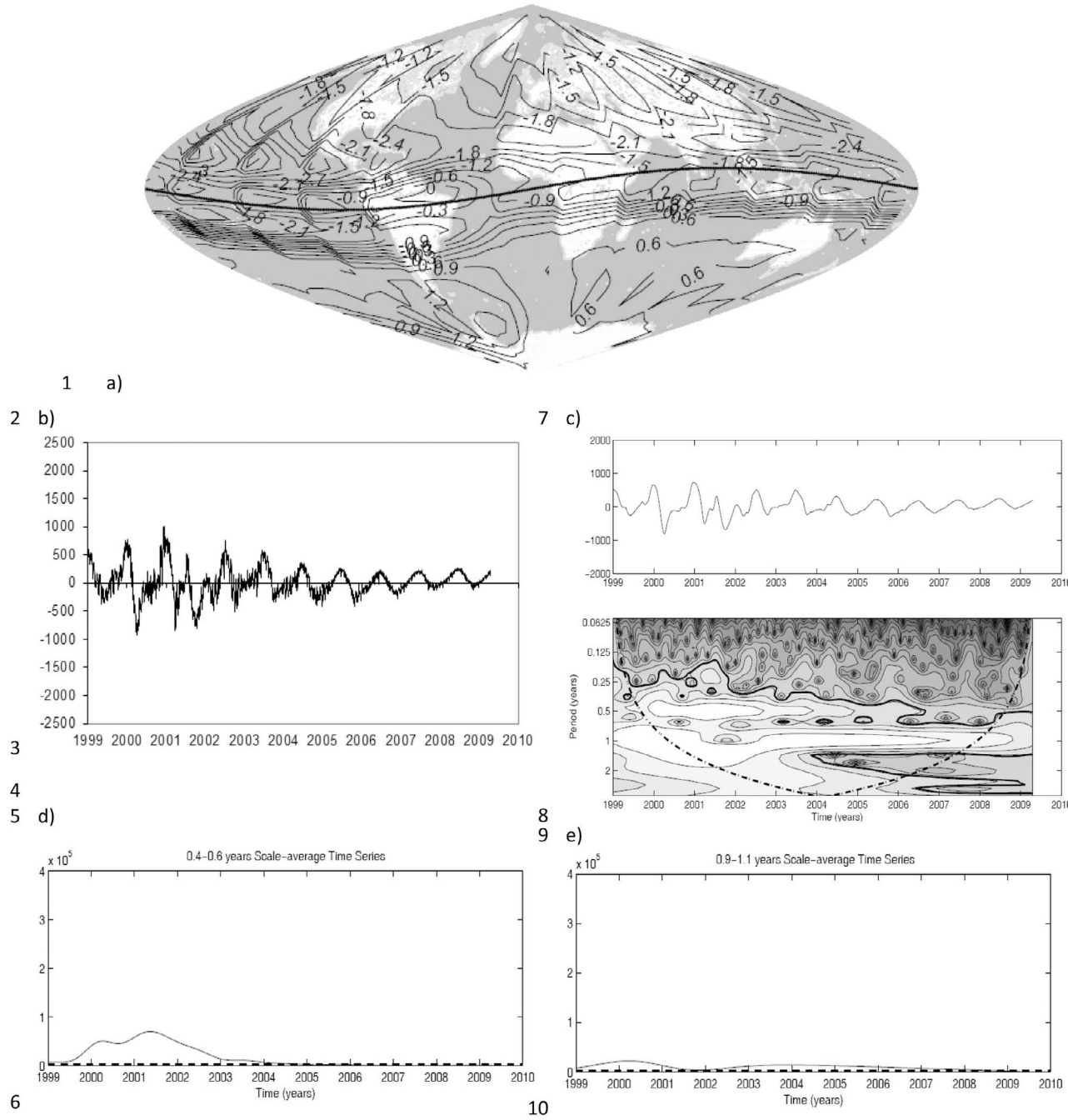

Figure 4. (a) Spatial variation in the second mode at night. (b) Time variation in the second mode at night. The *x* axis is the DOY and the *y* axis is the amplitude multiplied by a factor of 10^{-2}. (c) Wavelet power spectrum of the time variation residuals after mean Carrington period removal. (d) Scale-averaged wavelet power over the 0.4–0.6 year band. (e) Scale-averaged wavelet power over the 0.9–1.1 year band.

annual one and its maximum variability is recorded during high solar activity showing the same behavior than the mode 1 at nighttime. For low solar activity the annual component is stronger.

4. Conclusions

[39] The IGS ionospheric product, called IONEX file, provides very useful information to investigate the ionospheric anomalies. In this work we found a global distribution of the VTEC variability along 11 years (1999–2009). The PCA and wavelet techniques are numerical tools that improve the results interpretation. The former separate the main orthogonal component (called modes) of the VTEC scattering, and the second analyze the temporal variation of those components. For the study of winter and semiannual anomalies, which have different behaviors at different latitude, longitude and time, the combination of both techniques give us a complete and simple tool for interpretation of the VTEC

variability. Thus, it is easy to distinguish the anomalous effect focus of this work.

[40] The VTEC semiannual anomaly is globally recorded at noon especially at mid and low geomagnetic latitudes, which could be correlated with the electric dynamic processes in the low latitudes and much larger values are recorded in South American region probably related to the offset of the geomagnetic axis from the Earth spin axis in the Southern Hemisphere and the thermospheric circulation. This is in agreement with the results of *Millward et al.* [1996] using the CTIP model for N_mF_2.

[41] The amplitude of the semiannual variation has close relationship to the solar activity. At night the semiannual anomaly is found during high solar activity and the larger values are located at mid to low geomagnetic latitudes with maximum values also recorded in the South American region. Similar conclusions were reached by *Li and Yu* [2003].

[42] Either noon or night, there is a strong equinoctial asymmetry with values of VTEC in March equinox exceeding that of September equinox by up to 40% during high solar activity. Analogous results were found for N_mF_2 by *Balan et al.* [2000].

[43] At one hand, in agreement with *Zhao et al.* [2007], the winter anomaly is recorded at noon near the geomagnetic poles region.. This result verifies that the winter anomaly is strongly related to the change of composition which is closely related to the winter anomaly of (O/N_2) in this region [*Yu et al.*, 2006], being the lighter neutral constituents, which are formed in the summer hemisphere convected to the winter hemisphere.

[44] On the other hand, this anomaly is present at night during the ascending and descending phase and minimum of the solar cycle. These results confirm the findings of *Jakowski and Förster* [1995]. *Farelo et al.* [2002] analyzed the premidnight variability of N_mF_2 finding a seasonal dependence. It tends to be higher in winter than in summer at low geomagnetic latitudes. Our results show the NWA is larger at mid to low geomagnetic latitudes according to *Farelo et al.* [2002] with maximum values recorded in the South American region. The reason of the premidnight peaks in winter is due to a strong equatorward thermospheric wind raising the F_2 layer to heights with lower recombination rate [*Mikhailov et al.*, 2000].

[45] **Acknowledgments.** This research is supported by ANPCyT grant PICT 2007–00405, CONICET PIP 0130 and UNLP grant G095. The GPS-IONEX maps used in the present study were provided by the Jet Propulsion Laboratory online at ftp://cddisa.gsfc.nasa.gov/pub/gps/products/ionex/. Wavelet software was provided by C. Torrence and G. Compo, and it is available at http://atoc.colorado.edu/research/wavelets/. The authors are very grateful to the two anonymous reviewers, whose comments significantly enhanced the quality of this paper.

[46] Robert Lysak thanks the reviewers for their assistance in evaluating this paper.

References

Balan, N., Y. Otsuka, G. J. Bailey, S. Fukao, and M. A. Abdu (2000), Annual variations of the ionosphere: A review based on the MU radar observations, *Adv. Space Res.*, *25*, 153–162, doi:10.1016/S0273-1177(99)00913-8.

Chapman, S. (1931), The absorption and dissociatival or ionizing effect of monochromatic radiation in atmosphere on a rotating Earth, *Proc. Phys. Soc.*, *43*, 483–501, doi:10.1088/0959-5309/43/5/302.

Daubechies, I. (1992), *Ten Lectures on Wavelets*, *CBMS-NSF Reg. Conf. Ser. Appl. Math.*, vol. 61, Siam, Philadelphia, Pa.

Djurović, D., and P. Pâquet (1996), The common oscillations of solar activity, the geomagnetic field, and the Earth's rotation, *Sol. Phys.*, *167*, 427–439, doi:10.1007/BF00146351.

Farelo, A. F., M. Herraiz, and A. V. Mikhailov (2002), Global morphology of nighttime N_mF_2 enhancements, *Ann. Geophys.*, *20*, 1795–1802.

Farge, M. (1992), Wavelet transforms and their application to turbulence, *Annu. Rev. Fluid Mech.*, *24*, 393–457.

Feltens, J., and S. Schaer (1998), IGS products for the ionosphere, paper presented at IGS Analysis Center Workshop, Darmstadt, Germany, 9–11 Feb.

Ge, Z. (2007), Significance tests for the wavelet power and the wavelet power spectrum, *Ann. Geophys.*, *25*, 2259–2269, doi:10.5194/angeo-25-2259-2007.

Holschneider, M. (2000), Introduction to continuous wavelet analysis, in *Wavelets in the Geosciences*, *Lecture Notes Earth Sci.*, vol. 90, edited by R. Klees and R. H. N. Haagmans, pp. 1–71, Springer, Berlin.

Huang, Y.-N., and K. Cheng (1996), Solar cycle variations of the equatorial ionospheric anomaly in total electron content in the Asian region, *J. Geophys. Res.*, *101*, 24,513–24,520, doi:10.1029/96JA01297.

Jakowski, N., and M. Förster (1995), About the nature of the nighttime winter anomaly effect (NWA) in the *F* region of the ionosphere, *Planet. Space Sci.*, *43*, 603–612, doi:10.1016/0032-0633(94)00115-8.

Johnson, F. S. (1964), Composition changes in the upper atmosphere, in *Electron Density Distributions in the Ionosphere and Exosphere*, edited by E. Thrane, pp. 81–84, North-Holland, Amsterdam.

Kumar, P., and E. Foufoula-Georgiou (1994), Wavelet analysis in geophysics: An introduction, in *Wavelets in Geophysics*, edited by E. Foufoula-Georgiou and P. Kumar, pp. 1–43, Academic, San Diego, Calif.

Kumar, P., and E. Foufoula-Georgiou (1997), Wavelet analysis for geophysical applications, *Rev. Geophys.*, *35*(4), 385–412, doi:10.1029/97RG00427.

Lal, C. (1995), Correlation between the seasonal trends of planetary F2 layer ion density and intensity of the ring current, *J. Atmos. Sol. Terr. Phys.*, *57*, 45–49, doi:10.1016/0021-9169(93)E0022-2.

Lal, C. (2000), Sun-Earth geometry, geomagnetic activity, and planetary F2 layer ion density: Part I: Signatures of magnetic reconnection, *J. Atmos. Sol. Terr. Phys.*, *62*, 3–16, doi:10.1016/S1364-6826(99)00093-0.

Li, X., and T. Yu (2003), Annual and semi-annual variations of the observed f_0F_2 in a high solar activity year, *Terr. Atmos. Oceanic Sci.*, *14*(1), 41–62.

Ma, R., J. Xu, and H. Liao (2003), The features and a possible mechanism of semiannual variation in the peak electron density of the low latitude F2 layer, *J. Atmos. Sol. Terr. Phys.*, *65*, 47–57, doi:10.1016/S1364-6826(02)00192-X.

Mayr, H. G., and K. K. Mahajan (1971), Seasonal variation in the F_2 region, *J. Geophys. Res.*, *76*, 1017–1027, doi:10.1029/JA076i004p01017.

Mendillo, M., C.-L. Huang, X.-Q. Pi, H. Rishbeth, and R. R. Meier (2005), The global asymmetry in ionospheric total content, *J. Atmos. Sol. Terr. Phys.*, *67*, 1377–1387, doi:10.1016/j.jastp.2005.06.021.

Meza, A., and M. P. Natali (2008), Annual and semiannual TEC effects at low solar activity in midlatitude Atlantic region based on TOPEX, *J. Geophys. Res.*, *113*, D14115, doi:10.1029/2007JD009088.

Mikhailov, A. V., T. Y. Leschinkaya, and M. Förster (2000), Morphology of NmF2 nighttime increases in the Eurasian sector, *Ann. Geophys.*, *18*, 618–628, doi:10.1007/s00585-000-0618-5.

Millward, G. H., H. Rishbeth, T. J. Fuller-Rowell, A. D. Aylward, S. Quegan, and R. J. Moffett (1996), Ionospheric F_2 layer seasonal and semiannual variation, *J. Geophys. Res.*, *101*, 5149–5156, doi:10.1029/95JA03343.

Mursula, K., I. G. Usoskin, and B. Zieger (1997), On the claimed 5.5-year periodicity in solar activity, *Sol. Phys.*, *176*, 201–210, doi:10.1023/A:1004982203293.

Preisendorfer, R. W. (1988), *Principal Component Analysis in Meteorology and Oceanography*, 424 pp., Elsevier, Amsterdam.

Rishbeth, H., and C. S. G. K. Setty (1961), The F-layer at sunrise, *J. Atmos. Sol. Terr. Phys.*, *21*, 263–276.

Schaer, S., G. Beutler, and M. Rothacher (1998), Mapping and predicting the ionosphere, paper presented at IGS Analysis Center Workshop, Darmstadt, Germany, 9–11 Feb.

Torr, M. R., and D. G. Torr (1973), The seasonal behavior of the *F*2-layer of the ionosphere, *J. Atmos. Sol. Terr. Phys.*, *35*, 2237–2251, doi:10.1016/0021-9169(73)90140-2.

Torrence, C., and G. P. Compo (1998), A practical guide to wavelet analysis, *Bull. Am. Meteorol. Soc.*, *79*(1), 61–78, doi:10.1175/1520-0477(1998)079<0061:APGTWA>2.0.CO;2.

Ulrich, R. K., and J. E. Boyden (2006), Carrington coordinates and solar maps, *Sol. Phys.*, *235*, 17–29.

Unnikrishnan, K., R. B. Nair, and C. Venugopal (2002), Harmonic analysis and an empirical model for TEC over Palehua, *J. Atmos. Sol. Terr. Phys.*, *64*, 1833–1840, doi:10.1016/S1364-6826(02)00187-6.

Volland, H. (1969), The upper atmosphere as a multiple refractive medium for neutral air motions, *J. Atmos. Sol. Terr. Phys.*, *31*, 491–514, doi:10.1016/0021-9169(69)90002-6.

Vondrák, J. (1977), Problem of smoothing observational data II, *Bull. Astron. Inst. Czech.*, *28*, 84–93.

Wu, C. C., C. D. Fryb, J. Y. Liu, K. Lioud, and C. L. Tseng (2004), Annual TEC variation in the equatorial anomaly region during the solar minimum: September 1996–August 1997, *J. Atmos. Sol. Terr. Phys.*, *66*, 199–207, doi:10.1016/j.jastp.2003.09.017.

Yonezawa, T. (1971), The solar-activity and latitudinal characteristics of the seasonal, non-seasonal and semi-annual variations in the peak electron densities of the *F*2-layer at noon and at midnight in middle and low latitudes, *J. Atmos. Sol. Terr. Phys.*, *33*, 889–907, doi:10.1016/0021-9169(71)90089-4.

Yu, T., W. Wan, L. Liu, W. Tang, X. Luan, and G. Yang (2006), Analysis of global TEC annual and semi-annual variations by using IGS data, *Chin. J. Geophys.*, *49*(4), 841–847.

Zhao, B., W. Wan, L. Liu, T. Mao, Z. Ren, M. Wang, and A. B. Christensen (2007), Features of annual and semiannual variations derived form the global ionospheric maps of total electron content, *Ann. Geophys.*, *25*, 2513–2527, doi:10.5194/angeo-25-2513-2007.

L. I. Fernández, A. Meza, and M. P. Natali, Facultad de Ciencias Astronómicas y Geofísicas, Universidad Nacional de La Plata, Paseo del Bosque s/n, 1900 La Plata, Argentina. (paula@fcaglp.unlp.edu.ar)